



## 1        The long-term spatio-temporal variability of sea surface 2        temperature in the Northwest Pacific and the Near China Sea

3            **Zhiyuan Wu**<sup>1,2,3</sup>, **Changbo Jiang**<sup>1,3,\*</sup>, **Mack Conde**<sup>4</sup>, **Jie Chen**<sup>1,3</sup>, **Bin Deng**<sup>1,3</sup>

4            <sup>1</sup> School of Hydraulic Engineering, Changsha University of Science & Technology, Changsha, 410114,  
5            China

6            <sup>2</sup> School for Marine Science and Technology, University of Massachusetts Dartmouth, New Bedford,  
7            MA 02744, USA

8            <sup>3</sup> Key Laboratory of Water-Sediment Sciences and Water Disaster Prevention of Hunan Province,  
9            Changsha, 410114, China

10           <sup>4</sup> School of Marine Science and Ocean Engineering, University of New Hampshire, Durham, NH 03824,  
11           USA

12           \* Correspondence: chbjiang@csust.edu.cn

13           **Abstract:** The variability of the sea surface temperature (SST) in the Northwest Pacific has been studied  
14           on seasonal, annual and interannual scales based on the monthly datasets of ERSST 3b (1854-2017, 164  
15           years) and OISST V2 (1988-2017, 30 years). The overall trends, spatial-temporal distribution  
16           characteristics, regional differences in seasonal trends, and seasonal differences of SST in the Northwest  
17           Pacific have been calculated over the past 164 years based on these datasets. In the past 164 years, the  
18           SST in the Northwest Pacific has been increasing linearly year by year with a trend of 0.033 °C/10 yr.  
19           The period from 1880 to 1910 is a slow decreasing trend period in the past 164 years and the SST during  
20           the 1910-1930 period was a trough of the past 164 years. After 1930, SST has continued to increase until  
21           now. The increasing trend in the past 30 years has reached 0.132 °C/10 yr and the increasing trend in the  
22           past 10 years is 0.306 °C/10 yr, which is around ten times in the past 164 years. The SST in most regions  
23           of the Northwest Pacific showed a linear increasing trend year by year, and the increasing trend in the  
24           offshore region was stronger than that in the ocean and deep-sea region. The change trend of the SST in  
25           the Northwest Pacific shows a large seasonal difference, and the increasing trend in autumn and winter  
26           is larger than that in spring and summer. There are some correlations between the SST and some climate  
27           indexes and atmospheric parameters, the correlation between the SST and some atmospheric parameters  
28           have been discussed, such as NAO, PDO, SOI anomaly, TCW, Nino 3.4, SLP, Precipitation, T2 and wind  
29           speed. The lowest SST in the Near China Sea basically occurred in February and the highest in August.  
30           The SST fluctuation in the Bohai Sea and Yellow Sea (BYS) is the largest with a range from 5 °C to  
31           22 °C, the SST in the East China Sea (ECS) is from 18 °C to 27 °C, the smallest fluctuations occurs in  
32           the South China Sea (SCS) maintained at range of 26 °C to 29 °C. There are large differences between  
33           the mean and standard deviation in different sea regions.

34           **Keywords:** sea surface temperature; spatio-temporal distribution; interannual and interdecadal time  
35           scales; the Northwest Pacific



36 **1. Introduction**

37 The ocean is one of the important components of the ocean-atmosphere coupling system (Chelton  
38 and Xie, 2010; Wu et al., 2019a,b). Relative to the atmosphere, the ocean has characteristics such as slow  
39 change and large heat capacity (England et al., 2014). Because of the gradual changes in the ocean, climate  
40 change at the interannual, decadal, and longer timescales may be closely related to the ocean (Trenberth  
41 and Hurrell, 1994; Ault et al., 2009). The Sea Surface Temperature (SST) is the basis for the interaction  
42 between the ocean and the atmosphere (Wu et al., 2019c,d), and it characterizes the combined results of  
43 ocean heat (Buckley et al., 2014; Griffies et al., 2015), dynamic processes (Takakura et al., 2018). It is a  
44 very important parameter for climate change and ocean dynamics process, reflects sea-air heat and water  
45 vapor exchange. Observations and numerical simulations show that large-scale sea surface temperature  
46 anomalies of over 20° in longitude and latitude can cause significant changes in atmospheric circulation,  
47 such as the El Niño and La Niña phenomena (Chen et al., 2016; Zheng et al., 2016). During El Niño, the  
48 trade winds in the tropical East Pacific will be weakened, and the SST increased significantly, which was  
49 3~5°C higher than normal years. As a result, major changes have been made in the atmospheric  
50 circulation and ocean circulation, which has caused the worldwide atmospheric and marine environment  
51 and the abnormality of climate (Li et al., 2017).

52 The Northwest Pacific is particularly affected by the El Niño in the East Pacific and determines the  
53 oceanic climate change in China (Hu et al., 2018). On one hand, climate change causes an increasing SST  
54 in the northwestern Pacific, which increases the vertical stratification of the water, affects the atmospheric  
55 circulation, and changes the intensity and period of coastal winds and upwelling. On the other hand, the  
56 10-year periods Pacific Decadal Oscillation (PDO) and the El Niño-Southern Oscillation (ENSO) occur  
57 on average every 2 to 7 years, resulting in large variations in upwelling (Xiao et al., 2015; Yang et al.,  
58 2017; Xue et al., 2018). These factors will all lead to the impact on the marine environment in Chinese  
59 coastal areas, causing land-based droughts and floods and climate disasters (Xu et al., 2018). Therefore, it  
60 is very urgent to study the impact of climate change on SST in the Northwest Pacific and the Near China  
61 Sea. As one of the main parameters of global climate change and one of the important characterizations  
62 and predictors of El Niño, the study of SST changes is particularly important.

63 Previous scholars have done a lot of work on the changing trend of SST. According to the Fifth  
64 Assessment Report (AR5) of the Intergovernmental Panel on Climate Change (IPCC), the global SST  
65 warming trend was 0.064 °C/10 yr between 1880 and 2012 (Pachauri et al., 2014). In fact, many studies  
66 have shown that the Pacific SST anomalous changes are closely related to global and regional climate  
67 changes, and it has multi-scale temporal variations (Graham, 1994; Latif, 2006; Shakun and Shaman, 2009;  
68 Li et al., 2014). In addition, the El Niño-Southern Oscillation (ENSO) and the Pacific Decadal Oscillation  
69 (PDO), which are closely linked to global and regional climate change, are found in this area. Therefore,  
70 the Pacific is one of the key ocean areas that scholars have studied for a long time (Bao and Ren, 2014;  
71 Mei et al., 2015; Stuecker et al., 2015; Wills et al., 2018).

72 So far, two types of main meteorological SST datasets have been obtained: one based on measured  
73 mid-resolution (1° -5°) 100-year datasets and the other based on satellite high-resolution (1-10km) decade



74 datasets (Wang et al., 2011; Smith et al., 2014; Huang et al., 2015, 2016; Diamond et al., 2015). The former  
75 has rebuilt a time series of months over 150 years and the latter has accumulated over 30 years of time  
76 series on a daily average basis (Tian et al., 2019). The existing climatic datasets already have conditions  
77 for allowing the creation of a natural mode of change in SST in terms of duration and resolution (Liu et  
78 al., 2017; Wang et al., 2018). With the continuous improvement of ocean observation technology and the  
79 accumulation of satellite remote sensing data, the conditions for the scholars use the satellite data for short-  
80 term climate change research have been met. In recent years, the research and discussion on the interannual  
81 change of SST based on satellite remote sensing SST has attracted wide attention (Tang et al., 2003; Yang  
82 et al., 2013; Zhang et al., 2015; Skirving et al., 2018).

83 Satellite remote sensing can achieve large-area simultaneous measurements with high temporal and  
84 spatial resolution. The remote sensing SST obtained is conducive to a more comprehensive and rapid  
85 understanding of oceanographic phenomena that affect the ocean surface, including El Niño (Robinson,  
86 2016). At present, about 30 years of satellite remote sensing SST data have been accumulated (Franch et  
87 al., 2017), and a set of sea surface temperature data has been provided to study the conditions for the  
88 occurrence and development of ocean surface heat change modes in the temporal and spatial span and  
89 resolution. So, satellite remote sensing SST has received widespread attention in recent years.

90 At present, based on satellite remote sensing data, the time scales for the study of changes in SST in  
91 the Northwest Pacific, especially in the Near China Sea, are mostly within 20 years, which is relatively  
92 short for studying climate change (Song et al., 2018; Pan et al., 2018). Most of the space is targeted at  
93 specific local sea areas, and there is less research on the changes of the SST in the Northwest Pacific  
94 covering all marginal seas of China. Therefore, it is necessary to study the SST variation of large-scale  
95 and long-term sequences based on satellite remote sensing data.

96 Previous scholars have made great contributions to the study of global warming, but most of them  
97 are the overall changes in the regional average SST, and they tend to ignore the characteristics of changes  
98 in certain key sea areas. There are great differences in the trends of SST in different sea areas. The long-  
99 term trend of the SST changes in the Northwest Pacific (0° N- 60° N, 100° E- 180° E) over the past 164  
100 years (1854-2017) have been calculated based on the monthly datasets of ERSST 3b in this study. The  
101 temporal and spatial distribution characteristics of SST, the overall long-term sequence variation trend,  
102 the regional variation of the seasonal trend, and the seasonal differences were analyzed. The correlations  
103 with SST changes and climate parameters and indexes are been analyzed. To provide a reference for the  
104 study of global climate change, the characteristics of SST changes in the Near China Sea has been studied  
105 in this paper.

106 High spatial resolution SST datasets including average SST field and monthly SSTA field are been  
107 obtained. In view of the fact that there are many interannual and intra-annual changes, this paper analyzes  
108 the characteristics of SST changes based on these datasets. The trend, inter-decadal changes in SST and  
109 their causes, and the correlation with the climate parameters and indexes such as Nino-3.4 index are  
110 relatively low. The ocean thermal dynamic phenomenon is preliminarily discussed. The datasets are  
111 processed and analyzed to study the trend changes of the SST in the Northwest Pacific. To explore the

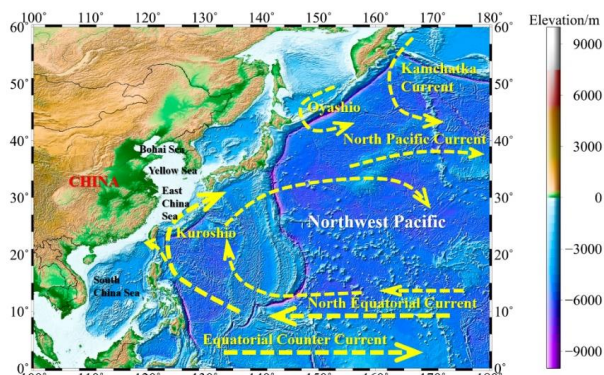


112 correlation and response mechanisms with climate systems such as the ENSO and the PDO, and to conduct  
113 a detailed analysis of typical sea areas.

## 114 **2. Study region, Data and Methods**

### 115 *2.1. Study Region*

116 The Northwest Pacific is the northwest region of the Pacific, are defined as the offshore region of  
117 0°N- 60°N and 100°E - 180°E in this study (Fig.1). There are more tropical cyclones over the Northwest  
118 Pacific than any other sea area in the world, with an average annual average of 35. About 80% of these  
119 tropical cyclones will develop into typhoons. On average, about 26 tropical cyclones per year reach at least  
120 the intensity of tropical storms, accounting for about 31% of the global tropical storms, and more than  
121 double the number of any other area. The sea-air interaction in this area is very strong and the change of  
122 SST is worth to explore.



123  
124 **Figure 1.** Bathymetric map of the Northwest Pacific and ocean circulation.

### 125 *2.2. SST Dataset*

126 Several data sources are used to analyze the long-term temporal and spatial variability of SST in the  
127 Northwest Pacific in this present study. Long-term statistics are based on the monthly SST data from the  
128 Extended Reconstructed Sea Surface Temperature (ERSST) 3b (1854-2017) (Smith et al., 2008). The  
129 ERSST dataset is a global monthly sea surface temperature analysis derived from the International  
130 Comprehensive Ocean-Atmosphere Dataset with missing data filled in by statistical methods. This  
131 monthly analysis begins in January 1854 continuing to the present (<https://www1.ncdc.noaa.gov/pub/data/cmb/ersst/v3b/>). The primary SST dataset analyzed in this study is the NOAA Optimum  
132 Interpolation (OI) Sea Surface Temperature (SST) V2 (OISST V2 1982-2017, <http://www.esrl.noaa.gov/psd/data/gridded/data.noaa.oisst.v2.html>) (Reynolds et al., 2002, 2007). The advantage of this dataset is  
133 apparent when compared with other gridded datasets such as HadISST, ERSST and OSTIA, which spans  
134 only the period since 2007.

135 The seasonal mean data are obtained by averaging the monthly average SST after the above-  
136 mentioned processing. The spring is March, April and May (MAM), the summer is June, July and August



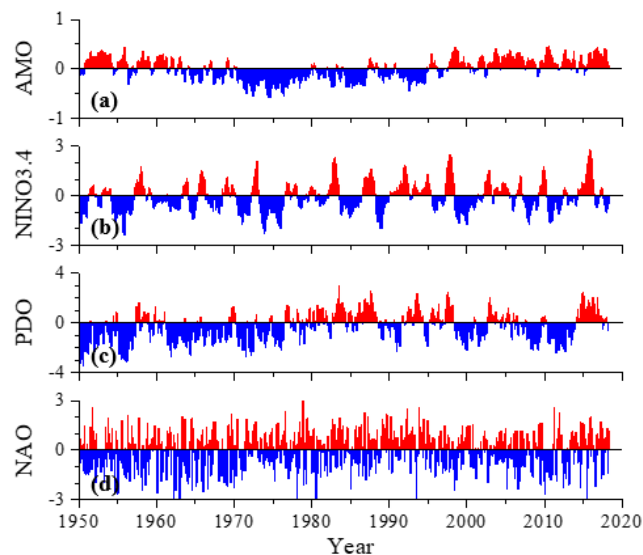
139 (JJA), the autumn is September, October and November (SON), and the winter is December of the  
140 previous year and January and February (DJF).

141 The SST anomaly is the deviation from the long-term SST average of the observations of the SST  
142 describing a particular area and time. The year anomaly represents the deviation of the average of the SST  
143 for a given year from the mean of the multi-year SST. The month anomaly represents the deviation of the  
144 average of the SST for a particular month from the average of the SST for that particular month for many  
145 years. In this paper, the mean value from 1854 to 2017 is taken as the climate mean state, and the sea  
146 surface temperature anomaly is subtracted from the SST field to obtain the SSTA field.

147 *2.3. Climate Index Dataset*

148 The Atlantic Multidecadal Oscillation (AMO) is a climate cycle that affects the sea surface  
149 temperature (SST) of the North Atlantic Ocean based on different modes on multidecadal timescales  
150 (<http://www.esrl.noaa.gov/psd/data/timeseries/AMO>, McCarthy et al, 2015). Niño 3.4 index uses SST to  
151 characterize ENSO, the Niño 3.4 SST region consists of temperature measurements from between 5° N -  
152 5° S and 120° - 170° W (Gergis and Fowler, 2005). The PDO index is the time coefficient of the first mode  
153 obtained by performing EOF of the mean SSTA in the north of 20° N in the North Pacific  
154 (<http://jisao.washington.edu/pdo/PDO.latest>). The North Atlantic Oscillation (NAO) is the most  
155 prominent modality in the North Atlantic. Its climate impact is most prominent mainly in North America  
156 and Europe, but it may also have an impact on the climate in other regions such as Asia. Recent studies  
157 have not only further confirmed its existence, but also revealed its connection with a wide range of oceans  
158 and atmospheric conditions.

159 The correlation between the SST and the atmospheric parameters is analyzed based on the ERA-  
160 Interim data. ERA-Interim refers to the European Centre for Medium-Range Weather Forecasts (ECMWF),  
161 which is an independent intergovernmental organization supported by 34 countries. Its goal is to develop  
162 numerical methods for mesoscale weather forecasting. The country provides forecasting services, conducts  
163 scientific and technological research to accumulate forecasts, and accumulates meteorological data. ERA-  
164 Interim is the latest global reanalysis product developed by ECMWF. The weather data and climate data  
165 from January 1988 to December 2017 are used in this paper, such as sea surface temperature, sea-to-air  
166 interface heat flux, and wind field data at a height of 10m, the spatial resolution of these datasets is  
167  $1.5^\circ \times 1.5^\circ$ .



168

169

170

**Figure 2.** AMO index (a), Niño 3.4 index (b), PDO index (c) and NAO index (d) during 1950~2017.

171 *2.4. Methods*

172 Regression analysis is an important part of mathematical statistics and multivariate statistics. It is a  
173 mathematical method to study the correlation between variables and variables. The regression analysis has  
174 a wide range of applications in the statistical forecasting of oceans and atmospheres. It is used to analyze  
175 the statistical relationship between a variable (called forecast) and one or more independent variables  
176 (called predict), and to establish a forecast. The regression equation produced by the quantity and forecast  
177 factor, and then based on this equation to make predictions of the forecast volume. Regression analysis  
178 includes linear regression and nonlinear regression. The linear regression is commonly used, and a linear  
179 regression analysis method is used in this paper.

180 Use  $x_i$  to represent a climate variable with a sample size of  $n$ . Use  $t_i$  to represent the time  
181 corresponding to  $x_i$  and establish a linear regression between  $x_i$  and  $t_i$ . The formula can be expressed as:

$$x_i = a + bt_i, \quad i = 1, 2, 3, \dots, n \quad (1)$$

182 Where,  $a$  is the regression constant and  $b$  is the regression coefficient.  $a$  and  $b$  can be calculated using  
183 the least squares method.

184 For the observation data  $x_i$  and the corresponding time  $t_i$ , the least-squares calculation result of the  
185 regression coefficient  $b$  and the constant  $a$  is expressed as:



$$b = \frac{\sum_{i=1}^n (x_i - \bar{x})(t_i - \bar{t})}{\sum_{i=1}^n (x_i - \bar{x})^2} \quad (2)$$

$$a = \bar{x} - b\bar{t}$$

186 The correlation coefficient between time  $t_i$  and  $x_i$  is:

$$r = \sqrt{\frac{\sum_{i=1}^n t_i^2 - \frac{1}{n} \left( \sum_{i=1}^n t_i \right)^2}{\sum_{i=1}^n x_i^2 - \frac{1}{n} \left( \sum_{i=1}^n x_i \right)^2}} \quad (3)$$

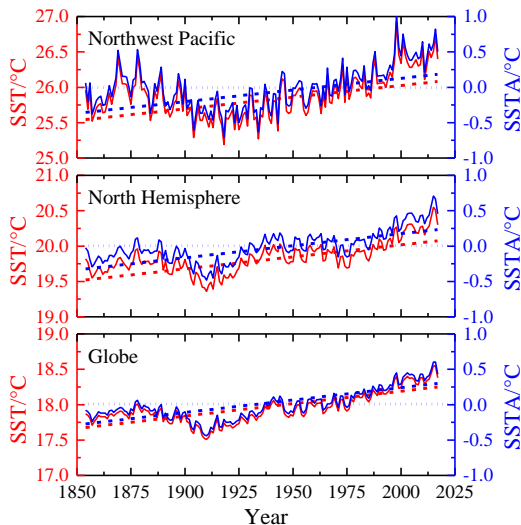
187 The correlation coefficient  $r$  is expressed as the degree of closeness of the linear correlation between  
188 the variable  $x$  and the time  $t$ . When  $r > 0$ ,  $b > 0$ , indicating that  $x$  increases with time  $t$ ; when  $r < 0$ ,  $b < 0$ ,  
189 indicating that the variable  $x$  decreases with time  $t$ . Perform a significant test on the correlation coefficient  
190 to determine the significance level  $\alpha$  (confidence is  $1 - \alpha$ ) first. If  $|r| > r_\alpha$ , shows that the trend of the  
191 variable  $x$  with time  $t$  is significant, otherwise it is not significant.

193 **3. Results and Discusses**

194 *3.1. Temporal distribution of SST*

195 With the gradual warming of the global climate, the average temperature of the ocean is also rising.  
196 In order to reflect the overall trend of SST in the Northwest Pacific over the past 164 years (1854-2017),  
197 the average monthly SST data from 1854 to 2017 was used. The time series curve of SST in the Northwest  
198 Pacific, the Northern Hemisphere, and the global ocean was obtained by processing, and the overall trend  
199 of the SST was analyzed, as shown in Fig. 3. As can be seen from the figure, SST in the different region  
200 have shown an increasing trend and SST has shown a significant increasing trend since the 20th century.

201 The SST datasets were used to calculate the SST anomaly time series and its linear variation trend in  
202 the Northwest Pacific, the Northern Hemisphere and the global ocean as shown in Fig. 3. The slope of the  
203 linear equation with one unknown obtained by least-squares fitting is the annual change rate of SST, as  
204 shown in Table 1. It shows the increasing trend of SST at different time scales. It can be seen that the data  
205 shows that the SST in the different region has shown a significant warming trend as a whole. It can be  
206 seen from Table 1 that from 1854 to 2017, the SST trend of Northwest Pacific, North Hemisphere and  
207 global ocean has increased by 0.033 °C to 0.035 °C per 10 years. In the past 50 years, the increasing rate  
208 of SST has reached 0.10 °C/10 yr or more, and the increasing rate in the last 10 years has reached 0.30°C.  
209 It can be seen that the warming trend of SST in the Northwest Pacific is very significant.



210

211

**Figure 3.** The temporal variability of annual SST.

212

**Table 1.** The average trend of SST (Unit: °C/10 yr).

	NWP	NH	GLO
1854-2017 (164yr)	0.033	0.034	0.035
1918-2017 (100yr)	0.100	0.059	0.069
1968-2017 (50yr)	0.128	0.128	0.102
1988-2017 (30yr)	0.132	0.149	0.102
2008-2017 (10yr)	0.306	0.379	0.274

213

NWP: Northwest Pacific; NH: North Hemisphere; GLO: Globe. All the trend is significant at  
214 the 95% confidence level.

215

There exist decadal to multi-decadal variations in the SST and SST anomalies series, with a general  
216 cool period from the 1880s to 1910s, a weak warm period from 1920s to 1940s, a weak cool period from  
217 1970s to 1980s, and a recent warm period from 1990s to present. Fig.3 also show that the interannual to  
218 decadal variability is larger in the Western Pacific, and it is smaller in the global ocean, indicating an  
219 increase in SST anomaly variability with the area. It is also interesting to note that the latest 10 years see  
220 a larger increasing trend of annual mean SST than that for the last 164 years, 100 years, 50 years and 30  
221 years, indicating an obvious speed-up of warming of the Northwest Pacific, North Hemisphere and globe  
222 ocean occurs in the last 10 years, and the growth rate over the past decade has been around ten times that  
223 of the past 164 years.

224

In the past 164 years, the correlation coefficient of SST trends in the Northwest Pacific was 0.73. It  
225 passed the 95% reliability test, which shows that the linear trend is significant, and the regression  
226 coefficient is 0.0033. This shows that in the past 164 years, the SST in the Northwest Pacific has been  
227 increasing linearly year by year at a rate of 0.033 °C/10 yr. It can be seen from Fig. 3 that during the period  
228 of 1870-1910, it showed a slowly decreasing trend, SST basically fluctuates slightly between 25.2 °C to



229 26.0 °C; during the period of 1910-1930, the SST is the valley of nearly 164 years, and the curve trend is  
230 also very gentle; after 1930, the SST oscillated gradually, and the trend has continued to this day.

231 In order to demonstrate the seasonal variation of the SST trend in the Northwest Pacific, the SST at  
232  $1^\circ \times 1^\circ$  at each grid point in the Northwest Pacific was averaged from 1854 to 2017 by winter, spring,  
233 summer, autumn and year in this study. The season-by-season linear trend of SST at each grid point has  
234 been analyzed. At the same time, the season-by-season time series of the SST anomalies were being  
235 calculated and the seasonal variation of the comparison trends was shown in Fig 4.

236 Fig.4 (a) and (b) show seasonal and annual mean SST and SST anomalies series. The blue lines are  
237 their trends of every seasonal mean SST and SST anomalies series for the Western Pacific during 1854-  
238 2017, the red lines is their trends during 1988-2017. The increasing trends during 1854-2017 is between  
239 0.032 °C/10 yr and 0.035 °C/10 yr for all seasons. The same as the annual pattern, seasonal pattern for the  
240 latest 30 years shows more significant warming trend than 164 years. Significant warming occurs in all  
241 seasons with those of autumn and winter being the largest, reaching 0.146 °C/10 yr and 0.124 °C/10 yr  
242 respectively at the last 30 years, and that of spring the smallest.

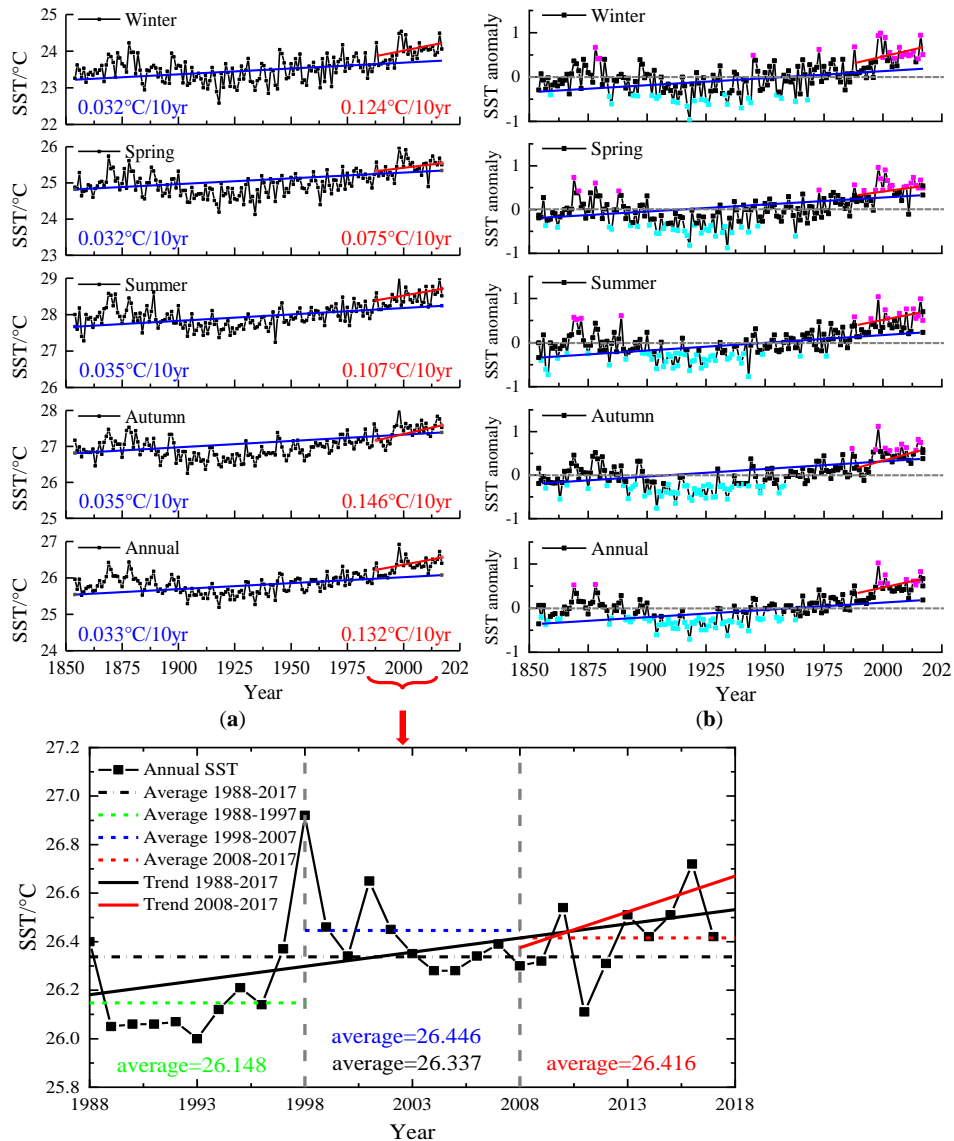
243 The magenta points mean the SST anomaly larger than 0.4 °C, and the cyan points mean the SST  
244 anomaly smaller than -0.4 °C in the Fig.4 (b). As can be seen from the figure, during the period from 1890  
245 to 1960, there were more negative anomalies and less than -0.4 °C, indicating that there was a cool period  
246 during this period. In the period from 1988 to 2017, there are more positive anomalies and more than  
247 0.4 °C, indicating that there is a warm period in the past 30 years.

248 In the analysis of the SST changes in the Northwest Pacific during the past 164 years, it has been  
249 found that there was a strong warming trend in SST over the past 30 years since 1988. It had been shown  
250 that the SST in the Northwest Pacific has an overall warming trend since the 1970s in the previous studies  
251 (Zhou et al., 2009; Kosaka et al., 2013) and this study. The time series curve of the SST in the Northwest  
252 Pacific from 1988 to 2017 was plotted as shown in Fig. 4(c).

253 Yamamoto's (1986) method has been used to determine the mutation point, and the formula is:

$$R_{SN} = \frac{|\bar{X}_1 - \bar{X}_2|}{S_1 + S_2} \quad (4)$$

254 Where,  $\bar{X}_1$ ,  $\bar{X}_2$ ,  $S_1$ ,  $S_2$  are the average and standard deviation of the two stages before and after  
255 the mutation year. It was found that there were six stations when  $X_1 = X_2 = 10$ ,  $R_{SN} \geq 0.7$  in 10 years before  
256 and after 1998/1999, and the significance level of the statistic reached  $\alpha = 0.05$ , according to which the  
257 SST was considered to have a mutation in this year. The difference between the mean value of the anomaly  
258 before and after the mutation was 0.30°C, and the similar results can also be seen in Fig. 4(c). It can be  
259 found that in the past 30 years, the SST in the Northwest Pacific has significantly warmed up as a whole.  
260 The highest annual mean SST appears in 1998, and the temperature undergoes a weak decreasing trend  
261 since then, but the average SST during 1998-2007 reaches 26.446 °C, which is higher than around 0.3 °C  
262 during 1988-1997. In the last 30 years of SST in the Northwest Pacific, the increasing trend in the last 10  
263 years is obviously greater than the trend in the last 30 years.



265

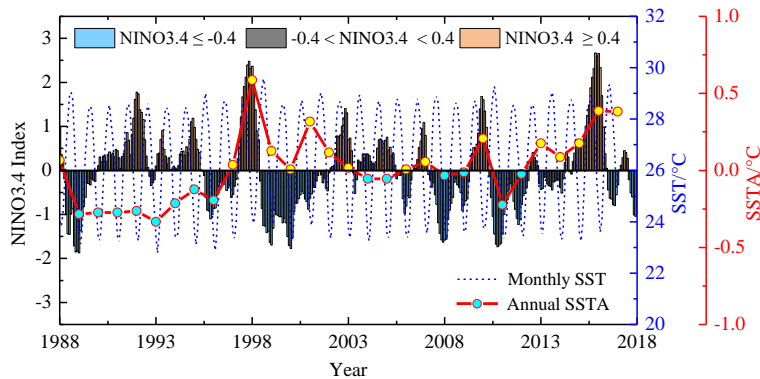
266 **Figure 4.** Variability of seasonal/annual SST. (a) the annual SST over the 1854-2017 period; (b)  
 267 the SST anomaly over the 1854-2017 period; (c) the SST over the 1988-2017 period (the latest  
 268 30 years).

269

270 The monthly average sea surface temperature in the Northwest Pacific is represented by an undulating  
 271 curve, as shown in the blue dashed line in Fig. 5, and the sea surface temperature anomaly is a red dotted  
 272 line. The positive value is filled in yellow, and the negative value is filled in cyan. The NINO3.4 index is  
 273 one of several El Niño/Southern Oscillation (ENSO) indicators based on sea surface temperatures.  
 NINO3.4 is the average sea surface temperature anomaly in the region bounded by 5°N to 5°S, from



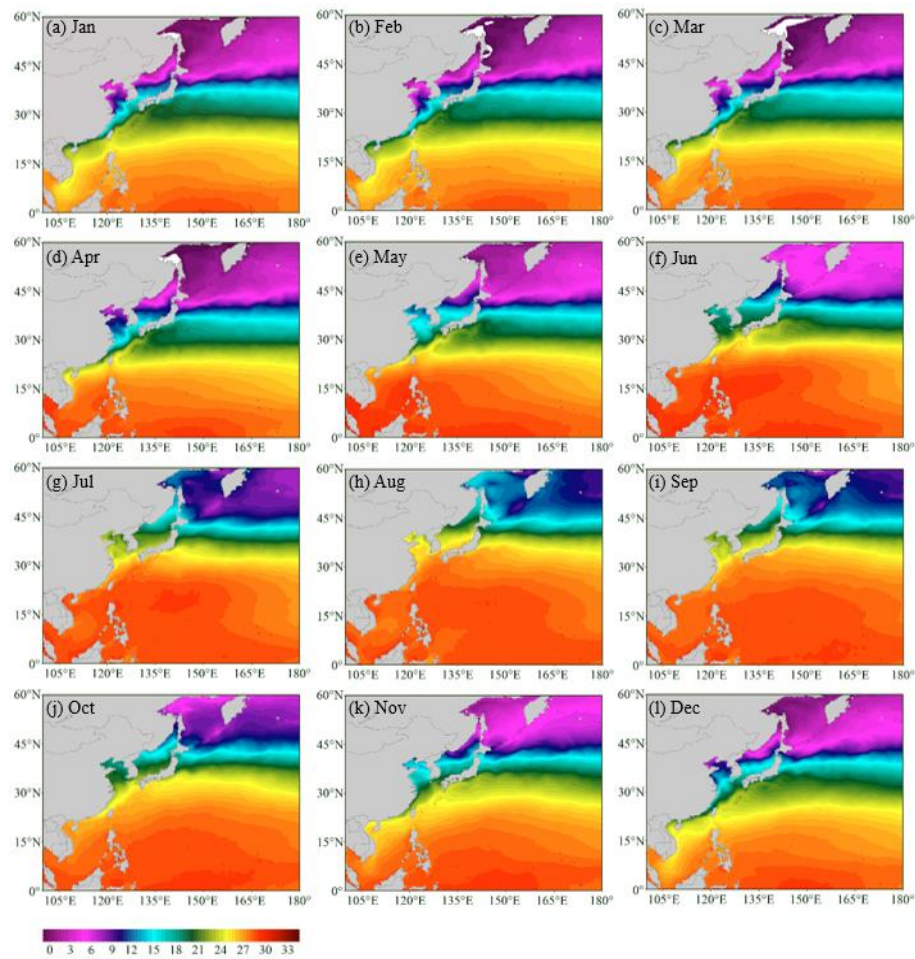
274 170°W to 120°W. This region has large variability on El Niño time scales, and is close to the region where  
275 changes in local sea surface temperature are important for shifting the large region of rainfall typically  
276 located in the far western Pacific. An El Niño or La Niña event is identified if the 5-month running-average  
277 of the NINO3.4 index exceeds +0.4°C for El Niño or -0.4°C for La Niña for at least 6 consecutive months.



278  
279 **Figure 5.** The Nino 3.4 index and SST/SSTA during 1988 to 2017. (El Niño in pink and La  
280 Niña in blue.).

281 It can be seen from Fig.5 that the SSTA minimum value point occurs in 1989 to 1996; the maximum  
282 value point occurs in 1998 and 2016, and the maximum year coincides with the El Niño year. It is shown  
283 that the anomalous changes of the SST in the Northwest Pacific are closely related to the occurrence year  
284 of ENSO. The changes of the SST in the Northwest Pacific are obviously affected by the anomalous  
285 changes of SST in the Equatorial Pacific. The average SSTA was basically negative before 1996, and the  
286 basic value after it was positive. That is, the average SSTA was generally lower than the average of 1988-  
287 2017 before 1996, and the average SSTA after 1996 was basically higher than the average of 1988-2017,  
288 which is also reflected in Fig. 4(c).

289 In the low-latitude region, SST is more evenly distributed along the latitudes in January to April and  
290 November to December, and are higher in the south and lower in the north. From May to October, the  
291 distribution of SST along the latitude is tilted, showing the distribution characteristics of higher in the  
292 southwest and lower in the northeast, which is affected by the ocean circulation. In addition, as can also  
293 be seen in Fig. 6, in the low-latitude region, the SST range of change in different months is relatively small,  
294 between 27 °C to 33 °C, the change range of 5 °C to 6 °C. In the high-latitude region, the SST can be less  
295 than 3 °C at the lowest, and greater than 15°C at the highest, with a relatively large variation of more than  
296 12 °C.

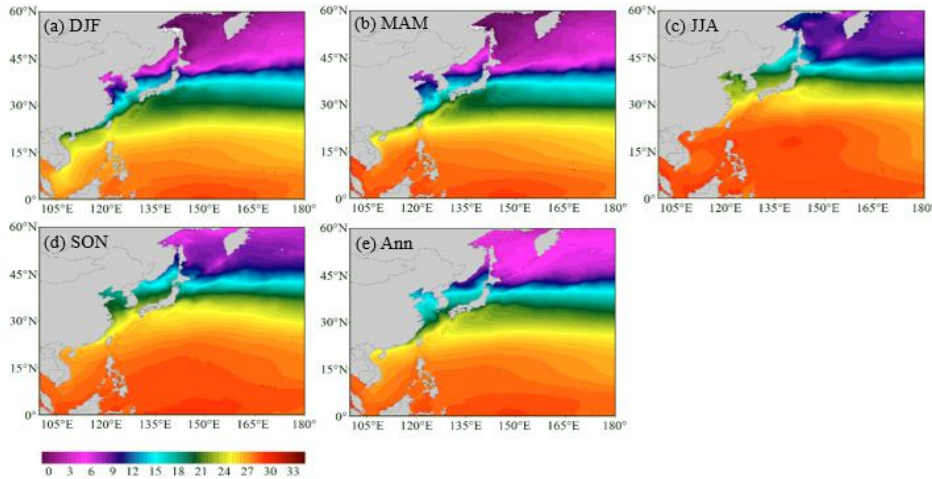


297

298

**Figure 6.** Spatial distribution of monthly SST over the 1988-2017 period.

299 Fig.7 shows the spatial distribution of seasonal and annual mean SST during the 1988-2017 period.  
300 As can be seen from the figure, the spatial distribution of average SST in each season and annual is similar,  
301 and similar to the monthly results (Fig. 6). In the low-latitude region, the SST is higher, but in the high  
302 latitudes. SST is relatively low. Annual mean SST decreases with increasing latitude, with high  
303 temperature ranging from 26°C to 28°C in the south and low temperature ranging from 3°C to 6°C in the  
304 north, which is closely related to the solar radiation distribution in the deep-sea region. The isotherm is  
305 northeast-southwest oriented and the SST gradient increases as getting closer to the mainland coastal line.  
306 It is obvious that the landmass effect in the winter time has contributed to the tilting of the isotherms,  
307 which was pointed out by Bao et al (2014).

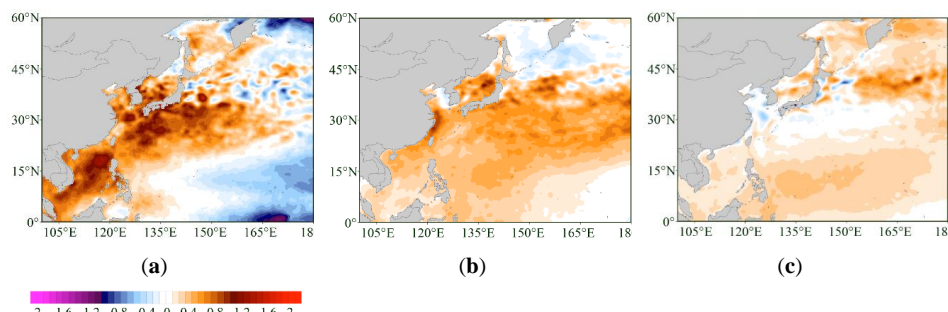


308

309 **Figure 7.** Spatial distribution of seasonal/annual SST over the 1988-2017 period (a) Winter:  
310 DJF; (b) Spring: MAM; (c) Summer: JJA; (d) Autumn: SON (e) Annual.

311 Fig. 8 shows the results of SST anomaly in three characteristic stages. Fig. 8(a) shows the SST  
312 anomaly for the annual 1998 minus 1988-2017, Fig. 8 (b) is the annual SST difference between the 10  
313 years after 1998 (1998-2007) and the previous 10 years (1988-1997) and Fig. 8 (c) is the SST anomaly for  
314 the last 10 years (2008-2017) and the past 30 years (1988-2017).

315 It can be seen that there was a significant positive anomaly across the past 30-year average in 1998  
316 from Fig. 8(a). The positive anomalies around 1.0°C are shown in a large area in the Near China Sea,  
317 indicating that the SST is significantly warmer. In the southeast and northeast of the Northwest Pacific,  
318 negative anomalies have occurred in this region, and the lowest is close to -0.6°C, indicating that the SST  
319 has cooled in this region. The SSTA in the Northwest Pacific showed a trend of high in the west and low  
320 in the east. From the previous analysis, we found that this mutation is highly coincident with El Niño (Fig.  
321 5). Therefore, it is likely that this phenomenon has been caused by the temperature difference and time  
322 difference caused by the transfer of high-temperature water in the Northeast Pacific to the Northwest  
323 Pacific.



324

325 **Figure 8.** (a) Ann 1998 minus 1988-2017; (b) Ann 1998-2007 minus 1988-1997; (c) Ann 2008-  
326 2017 minus 1988-2017.



327 It can be seen from Fig. 8(b) that the SST during the 10 years from 1998 to 2007 has significantly  
328 increased compared with the previous 10 years from 1988 to 1997. The positive anomaly occurs to be  
329 0.4°C to 0.8°C in the south region of 40° N. In the 10 years since 1998, the SST in the region has increased  
330 by 0.4°C to 0.8°C over the previous 10 years. In the region between 45° N and 60° N, the effect is small  
331 and is maintained between -0.2°C and 0°C, indicating that the SST in this region has not changed  
332 substantially or slightly.

333 Fig. 8(c) shows the anomalous results of SST over the last 10 years (2008-2017) and relatively nearly  
334 30 years (1988-2017). As can be seen from the figure, in addition to the Bohai Sea, the Yellow Sea, and  
335 the southern region of Japan, there is a wide range of positive anomaly in other regions, and the past 10  
336 years have increased on average in the past 30 years. From Fig. 4(a) and (b), we have known that the  
337 increasing trend of SST over the past 30 years is around three to four times that of the rising trend of SST  
338 over the past 164 years. Therefore, the increasing trend of SST in the past 10 years is more significant,  
339 which is consistent with the results in Fig. 4(c) and Table 1.

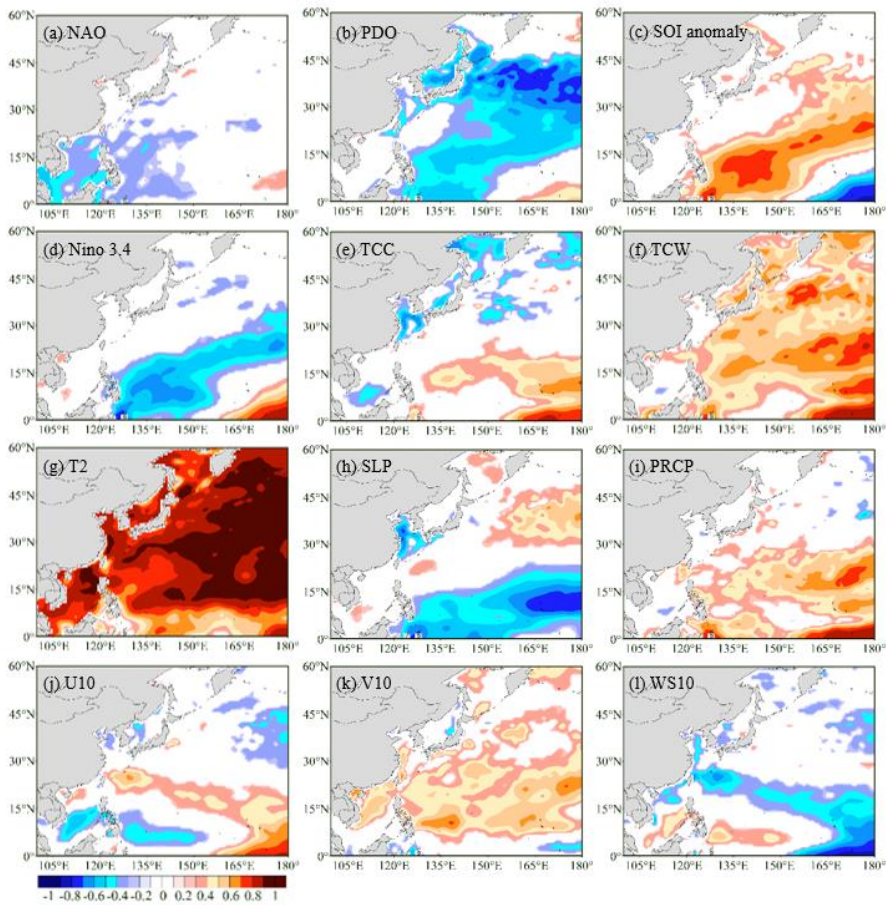
340 *3.3. Correlation between the SST and the atmospheric parameters*

341 Based on monthly data from ERA-Interim, there is some correlation between SST and atmospheric  
342 parameters have been shown in Fig. 9, all marked patterns are at the level of significance equal to 0.05. It  
343 can be seen from Fig. 9(a) that there is a non-significant correlation between SST and North Atlantic  
344 Oscillation (NAO), but in the South China Sea and around the region. It shows a weak negative correlation  
345 between South China Sea SST and NAO. The Pacific Decadal Oscillation (PDO) is an important factor of  
346 climate change of the Northwest Pacific, and it has a strong correlation with ENSO. The PDO has a great  
347 influence on the Asian monsoon and climate change in the Northwest Pacific and is closely related to  
348 ENSO. There is a significant negative correlation between SST and PDO can be seen from Fig. 9(b). The  
349 Niño-3.4 index is usually used to indicate the intensity of the El Niño/La Niña event. So there is a  
350 significant negative correlation between SST and the atmospheric parameters Nino 3.4 in Fig. 9(d).

351 There is a significant positive correlation between SST and the Southern Oscillation Index (SOI) in  
352 Fig. 9(c), which is a standardized index based on the observed sea level pressure differences between  
353 Tahiti and Darwin, Australia. The monthly correlation between SST and T2 is high throughout the study  
354 region, most markedly ( $R>0.95$ ) over all Northwest Pacific. The effect of T2 on SST is significant over  
355 98% of the study region in all seasons. This is in good agreement with the previous studies (Skliris et al,  
356 2012; Shaltout and Omstedt, 2014). Similarly, based on monthly data, there is a significant positive  
357 correlation between SST and Total Column Water (TCW), precipitation (PRCP).

358 The maximum negative correlation between the effect of Wind Speed 10m (WS10) on SST occurs  
359 southeast Northwest Pacific, and significant in an only small region. However, the direct correlation  
360 between V10 and SST is significant and positive over more of the Northwest Pacific.

361



362

363 **Figure 9.** The correlation coefficient between SST and the atmospheric components. (level of  
364 significance equal to 0.05).

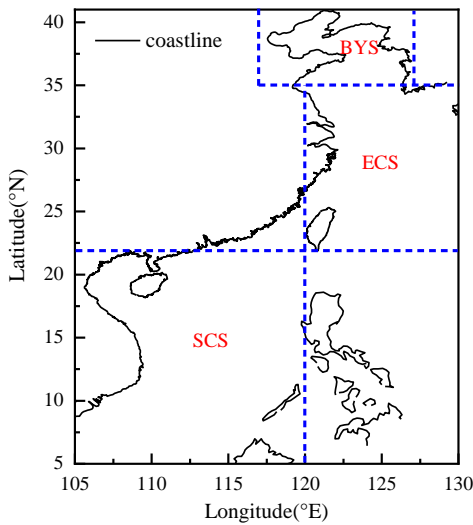
365 *3.4. The Near China Sea SST characteristics*

366 The Near China Sea is defined as the four sea areas of the Bohai Sea, Yellow Sea, East China Sea,  
367 and South China Sea, and include the Kuroshio Extension, the part of Northwest Pacific and the sea  
368 surrounding Japan in this study, which defined as the offshore region of 5°N-41°N and 105°E-130°E. The  
369 changes in the average SST in the Yellow Sea and the Bohai Sea are very similar, so we analyze the two  
370 sea areas together. Therefore, the region is further divided into three sub-regions: Bohai Sea and Yellow  
371 Sea (BYS, 35°N-41°N and 117°E-127°E), East China Sea (ECS, 22°N-35°N and 120°E-130°E) and South  
372 China Sea (SCS, 5°N-22°N and 105°E-120°E)<sup>25</sup>.

373 Fig.11 shows the spatial distribution of seasonal and annual mean SST in the Near China Sea during  
374 the 1988-2017 period. Annual mean SST decreases with increasing latitude, with high temperature ranging  
375 from 26°C to 28°C in the south and low temperature ranging from 14°C to 16°C in the north, which is

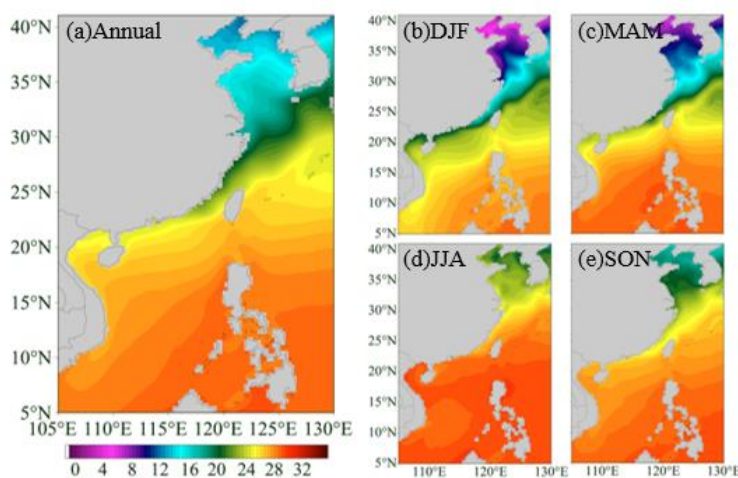


376 closely related to the solar radiation distribution in the offshore region. The isotherm is northeast–  
377 southwest oriented and the SST gradient increases as getting closer to the mainland coastal line. It is  
378 obvious that the landmass effect in the winter has contributed to the tilting of the isotherms, which was  
379 pointed out by Bao et al.<sup>25</sup>. The ECS exhibits the largest temperature gradient, and the SCS in the tropical  
380 zone the lowest temperature gradient.



381

382 **Figure 10.** Study regions defined in this paper. BYS: the Bohai Sea and the Yellow Sea; ECS:  
383 the East China Sea; SCS: the South China Sea.



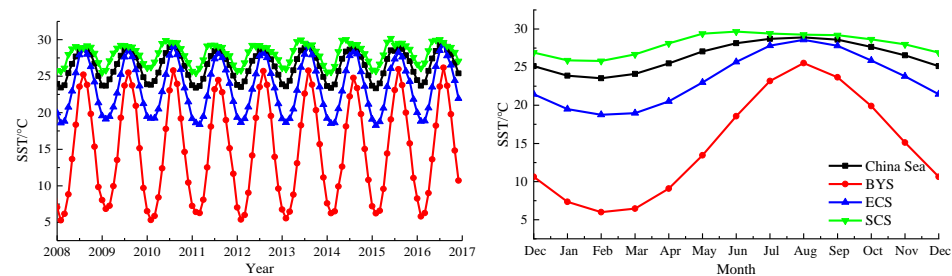
384

385 **Figure 11.** Annual (left) and seasonal (right) mean SST distribution during 1988-2017 in the  
386 China Sea. (a) Annual; (b) Winter: DJF; (c) Spring: MAM; (d) Summer: JJA; (e) Autumn: SON.



387 The monthly mean surface temperature changes over the past 10 years in the three regions (BYS,  
388 ECS and SCS) and the whole sea area (China Sea) are shown in Fig. 12. Fig. 12(a) shows the year-by-year  
389 variation of SST in different regions in the last 10 years, and Fig. 12(b) shows the monthly SST variations  
390 in different regions in the past 10 years. The change variability of SST in different regions are basically  
391 synchronized. The minimum temperature basically occurs in February and the warmest occurs in August.  
392 The fluctuation range of SST in BYS is the largest, basically between 5 °C to 22 °C, from 18 °C to 27 °C  
393 in the East China Sea, and the smallest fluctuations is in the South China Sea, maintained at a range of  
394 26 °C to 29 °C. There are large differences between the mean and standard deviation in different regions.

395



396

397 **Figure 12.** Long term monthly mean SST of the marginal seas of China during 2008-2017 (a)  
398 Yearly; (b) Monthly. Black line: China Sea; red line: Bohai Sea and Yellow Sea (BYS); blue  
line: East China Sea (ECS); green line: South China Sea (SCS).

399

400 Table 2 shows the annual and seasonal SST characteristics of the study area Near China Sea based  
401 on monthly data from 1988 to 2017. It can be found that in addition to the winter and spring in the BYS,  
402 the SST in each season of other regions shows an increasing trend from the table. Average increasing  
403 trends of SST during 1988 to 2017 in BYS is 0.015 °C/ 10yr, 0.14 °C/ 10yr for the ECS, 0.12 °C/ 10yr for  
404 the SCS and 0.12 °C/ 10yr for whole Near China Sea respectively, and all the trends are significant at the  
405 99% confidence level. From the point of average annual SST, the SST in the South China Sea is the highest,  
406 reaching 28.01°C, followed by the East China Sea with 23.4°C, the lowest in the Bohai Sea and the Yellow  
407 Sea is 14.98°C, and the SST in the whole Near China Sea is 26.4°C. Table 3 shows the peak value and  
408 time of the annual and seasonal SST of the study area Near China Sea based on monthly data from 1988  
409 to 2017. In the past 30 years, colder SST occurs in 1989, 1990, 1992, 1993, 2003, 2008, 2010, 2011.  
410 Warmer SST occurs in 1997, 1998, 1999, 2001, 2015, 2016.



411 **Table 2.** Annual and seasonal SST characteristics of the study area Near China Sea based on  
 412 monthly data from 1988 to 2017.

	Average trend (°C/10yr)					Average (°C) ± standard deviation				
	Winter	Spring	Summer	Autumn	Annual	Winter	Spring	Summer	Autumn	Annual
BYs	-0.027	-0.097	0.084	0.13	<b>0.015</b>	8.08 ± 0.52	9.84 ± 0.49	22.44 ± 0.54	19.56 ± 0.44	<b>14.98 ± 0.34</b>
ECS	0.11	0.04	0.15	0.23	<b>0.14</b>	19.81 ± 0.33	20.87 ± 0.35	27.24 ± 0.31	25.66 ± 0.34	<b>23.40 ± 0.26</b>
SCS	0.13	0.10	0.11	0.14	<b>0.12</b>	26.09 ± 0.33	28.02 ± 0.27	29.38 ± 0.28	28.54 ± 0.27	<b>28.01 ± 0.23</b>
Whole	0.13	0.08	0.11	0.16	<b>0.12</b>	24.07 ± 0.27	25.53 ± 0.25	28.50 ± 0.24	27.50 ± 0.26	<b>26.40 ± 0.21</b>

413 **Table 3.** Peak value and time of the annual and seasonal SST of the study area Near China Sea  
 414 based on monthly data from 1988 to 2017.

	Minimum (°C) and time (yr)					Maximum (°C) and time (yr)				
	Winter	Spring	Summer	Autumn	Annual	Winter	Spring	Summer	Autumn	Annual
BYs	7.13 (2003)	8.88 (2010)	21.13 (1993)	18.69 (1992)	14.45 (2010)	9.17 (2001)	11.02 (1998)	23.99 (1997)	20.70 (1998)	15.85 (1998)
ECS	19.30 (1989)	20.04 (2011)	26.76 (1993)	25.01 (1992)	22.97 (1993)	20.54 (1999)	21.84 (1998)	28.06 (2016)	26.43 (1998)	24.14 (1998)
SCS	25.53 (1993)	27.50 (2011)	28.97 (2008)	27.98 (1992)	27.68 (1989)	26.78 (2016)	28.53 (2001)	30.02 (1998)	29.14 (2015)	28.58 (1998)
Whole	23.61 (1993)	24.99 (2011)	28.18 (1990)	26.94 (1992)	26.07 (1993)	24.63 (1999)	26.05 (1998)	29.09 (1998)	28.18 (1998)	26.98 (1998)

415 **4. Conclusions**

416 The Northwest Pacific sea surface variability is affected by a combination of oceanic and atmospheric  
 417 processes and displays significant regional and seasonal behavior. Monthly SST datasets based on ERSST  
 418 3b (1854-2017, 164 years) and OISST V2 (1988-2017, 30 years) are used to make some long-term  
 419 temporal and spatial variability statistics. The following conclusions can be drawn from the analysis.

420 In the last 164 years, SST in the Northwest has gradually increased, with an increasing trend of  
 421 0.033 °C/10 yr. Especially in the past 30 years, the increasing trend of SST reaches to 0.132 °C/10 yr, and  
 422 the increasing trend of SST reaches to 0.306 °C/10 yr in the last 10 years, which increasing trend is very  
 423 obviously. The trend of the SST varies seasonally. The increasing trend in winter and autumn are  
 424 0.124 °C/10 yr and 0.146 °C/10 yr respectively, which are greater than spring and summer, with  
 425 0.075 °C/10 yr and 0.107°C /10 yr respectively. There was an SST mutation point occurred around 1998,  
 426 the average annual SST for the 10 years after 1998 increased by 0.3°C over the previous 10 years. It has  
 427 been found that the change of SST/SSTA in the Northwest Pacific is closely related to the ENSO through  
 428 the statistical analysis of Nino3.4 index and SST/SSTA.



429 From the perspective of spatial distribution, the annual mean SST decreases with increasing latitude  
430 in conclusion, with high temperature ranging from 27°C to 33°C in the south and low temperature ranging  
431 from 3°C to 15°C in the north. The SST is higher in the low-latitude (near equator) region and lower in  
432 the high-latitude region. In the low-latitude region, SST is more evenly distributed along the latitudes in  
433 November to April, but from May to October, the distribution of SST along the latitude is tilted, showing  
434 the distribution characteristics of higher in the southwest and lower in the northeast, which is affected by  
435 the ocean circulation.

436 There are many correlations between the SST and some climate indexes and atmospheric parameters,  
437 such as Pacific Decadal Oscillation (PDO), Southern Oscillation Index (SOI), Nino 3.4, total water vapor  
438 column (TWC), temperature at 2 meters (T2), sea level pressure (SLP), precipitation (PRCP) and wind  
439 speed at 10 meters (U10, V10 and WS10). A very significant positive correlation between SST and T2,  
440 TWC was been found, of which the correlation coefficient between SST and T2 exceeded 98%. PDO,  
441 Nino 3.4 is negatively correlated with SST, and the correlation between other indexes and parameters and  
442 SST is weak.

443 The whole Near China Sea was divided into three sections to analysis its spatial variability in a  
444 different region, which is the Bohai Sea and Yellow Sea (BYS), East China Sea (ECS) and South China  
445 Sea (SCS). The SST in the BYS is coolest with a range from 5 °C to 22 °C, and the warmest in the SCS  
446 with a range from 26 °C to 29 °C. It can be seen from the statistical data that in addition to the winter and  
447 spring in the BYS, SST in other regions and time had shown a warming trend. In the past 30 years, the  
448 trend of SST increase of BYS was 0.015 °C/10 yr, while that of ECS and SCS was 0.14 °C/10 yr and  
449 0.12 °C/10 yr, respectively.

450 **Competing interests:** The authors declare that they have no conflict of interest.

451 **Financial support:** The study was supported by the National Natural Science Foundation of China  
452 (Grant Nos. 51809023, 51839002 and 51879015).

453 **References:**

454 Ault, T. R., Cole, J. E., Evans, M. N., Barnett, H., Abram, N. J., Tudhope, A. W., and Linsley., B. K.:  
455 Intensified decadal variability in tropical climate during the late 19th century, *Geophysical Research  
456 Letters*, 36, L08602, <https://doi.org/10.1029/2008GL036924>, 2009.

457 Bao, B., and Ren, G.: Climatological characteristics and long-term change of SST over the marginal seas  
458 of China, *Continental Shelf Research*, 77, 96-106, <https://doi.org/10.1016/j.csr.2014.01.013>, 2014.

459 Buckley, M. W., Ponte, R. M., Forget, G., and Heimbach, P.: Low-frequency SST and upper-ocean heat  
460 content variability in the North Atlantic, *Journal of Climate*, 27, 4996-5018,  
461 <https://doi.org/10.1175/JCLI-D-13-00316.1>, 2014.

462 Chelton, D. B., and Xie, S. P.: Coupled ocean-atmosphere interaction at oceanic mesoscales,  
463 *Oceanography*, 23, 52-69, <https://doi.org/10.5670/oceanog.2010.05>, 2010.



464 Chen, Z., Wen, Z., Wu, R., Lin, X., and Wang, J.: Relative importance of tropical SST anomalies in  
465 maintaining the Western North Pacific anomalous anticyclone during El Niño to La Niña transition  
466 years, *Climate dynamics*, 46, 1027-1041, <https://doi.org/10.1007/s00382-015-2630-1>, 2016.

467 Diamond, M. S., and Bennartz, R.: Occurrence and trends of eastern and central Pacific El Niño in different  
468 reconstructed SST data sets, *Geophysical Research Letters*, 42, 10375–10381,  
469 <https://doi.org/10.1002/2015GL066469>, 2015.

470 England, M. H., McGregor, S., Spence, P., Meehl, G. A., Timmermann A., Cai W., Gupta A. S., McPhaden  
471 M. J., Purich A., and Santoso A.: Recent intensification of wind-driven circulation in the Pacific and  
472 the ongoing warming hiatus, *Nature Climate Change*, 4, 222, <https://doi.org/10.1038/nclimate2106>,  
473 2014.

474 Franch, B., Vermote, E.F., Roger, J.-C., Murphy, E., Becker-Reshef, I., Justice, C., Claverie, M., Nagol,  
475 J., Csiszar, I., Meyer, D., Baret, F., Masuoka, E., Wolfe, R., and Devadiga, S.: A 30+ Year AVHRR  
476 Land Surface Reflectance Climate Data Record and Its Application to Wheat Yield Monitoring,  
477 *Remote Sensing*, 9, 296, <https://doi.org/10.3390/rs9030296>, 2017.

478 Gergis, J. L., and Fowler, A. M.: Classification of synchronous oceanic and atmospheric El Niño-Southern  
479 Oscillation (ENSO) events for palaeoclimate reconstruction, *International Journal of Climatology*,  
480 25, 1541-1565, <https://doi.org/10.1002/joc.1202>, 2005.

481 Graham, N. E.: Decadal-scale climate variability in the tropical and North Pacific during the 1970s and  
482 1980s: Observations and model results, *Climate Dynamics*, 10, 135-162,  
483 <https://doi.org/10.1007/BF00210626>, 1994.

484 Griffies, S. M., Winton, M., Anderson, W. G., Benson, R., Delworth, T. L., Dufour, C. O., Dunne, J. P.,  
485 Goddard, P., Morrison, A. K., Rosati, A., Wittenberg, A. T., Yin, J., and Zhang R.: Impacts on ocean  
486 heat from transient mesoscale eddies in a hierarchy of climate models, *Journal of Climate*, 28, 952-  
487 977, <https://doi.org/10.1175/JCLI-D-14-00353.1>, 2015.

488 Hu, H., Wu, Q., and Wu, Z.: Influences of two types of El Niño event on the Northwest Pacific and tropical  
489 Indian Ocean SST anomalies, *Journal of Oceanology and Limnology*, 36, 33-47,  
490 <https://doi.org/10.1007/s00343-018-6296-5>, 2018.

491 Huang, B., Banzon, V. F., Freeman, E., Lawrimore, J., Liu, W., Peterson, T. C., Smith, T. M., Thorne, P.  
492 W., Woodruff S. D., and Zhang, H. M.: Extended reconstructed sea surface temperature version 4  
493 (ERSST. v4). Part I: upgrades and intercomparisons, *Journal of climate*, 28, 911-930,  
494 <https://doi.org/10.1175/JCLI-D-14-00006.1>, 2015.

495 Huang, B., Thorne, P. W., Smith, T. M., Liu, W., Lawrimore, J., Banzon, V. F., and Menne, M. Further  
496 exploring and quantifying uncertainties for extended reconstructed sea surface temperature (ERSST)  
497 version 4 (v4), *Journal of Climate*, 29, 3119-3142, <https://doi.org/10.1175/JCLI-D-15-0430.1>, 2016.

498 Kosaka, Y., and Xie, S. P.: Recent global-warming hiatus tied to equatorial Pacific surface cooling, *Nature*,  
499 501, 403, <https://doi.org/10.1038/nature12534>, 2013.

500 Latif, M.: On North Pacific multidecadal climate variability, *Journal of climate*, 19, 2906-2915,  
501 <https://doi.org/10.1175/JCLI3719.1>, 2006.



502 Li, G., Li, C., Tan, Y., and Bai, T.: The interdecadal changes of south pacific sea surface temperature in  
503 the mid-1990s and their connections with ENSO, *Advances in Atmospheric Sciences*, 31, 66-84,  
504 <https://doi.org/10.1007/s00376-013-2280-3>, 2014.

505 Li, X., Zong, Y., Zheng, Z., Huang, G., and Xiong, H.: Marine deposition and sea surface temperature  
506 changes during the last and present interglacials in the west coast of Taiwan Strait, *Quaternary  
507 International*, 440, 91-101, <https://doi.org/10.1016/j.quaint.2016.05.023>, 2017.

508 Liu, C., Sun, Q., Xing, Q., Liang, Z., Deng, Y., and Zhu, L.: Spatio-temporal variability in sea surface  
509 temperatures for the Yellow Sea based on MODIS dataset, *Ocean Science Journal*, 52, 1-10,  
510 <https://doi.org/10.1007/s12601-017-0006-7>, 2017.

511 McCarthy, G. D., Haigh, I. D., Hirschi, J. J. M., Grist, J. P., and Smeed, D. A.: Ocean impact on decadal  
512 Atlantic climate variability revealed by sea-level observations, *Nature*, 521, 508,  
513 <https://doi.org/10.1038/nature14491>, 2015.

514 Mei, W., Xie, S. P., Primeau, F., McWilliams, J. C., and Pasquero, C.: Northwestern Pacific typhoon  
515 intensity controlled by changes in ocean temperatures, *Science Advances*, 1, e1500014,  
516 <https://doi.org/10.1126/sciadv.1500014>, 2015.

517 Pachauri, R. K., Allen, M. R., Barros, V. R., Broome, J., Cramer, W., Christ, R., Church, J. A., Clarke, L.,  
518 Dahe, Q., Dasgupta, P., Dubash, N. K., et al.: Climate Change 2014: Synthesis Report. Contribution  
519 of Working Groups I, II and III to the Fifth Assessment Report of the Intergovernmental Panel on  
520 Climate Change / R. Pachauri and L. Meyer (editors), Geneva, Switzerland, IPCC, ISBN: 978-92-  
521 9169-143-2, 2014.

522 Pan, X., Wong, G. T., Ho, T. Y., Tai, J. H., Liu, H., Liu, J., and Shiah, F. K.: Remote sensing of surface  
523 [nitrite+ nitrate] in river-influenced shelf-seas: The northern South China Sea Shelf-sea, *Remote  
524 Sensing of Environment*, 210, 1-11, <https://doi.org/10.1016/j.rse.2018.03.012>, 2018.

525 Reynolds, R. W., Rayner, N. A., Smith, T. M., Stokes, D. C., and Wang, W.: An improved in situ and  
526 satellite SST analysis for climate, *Journal of climate*, 15: 1609-1625, [https://doi.org/10.1175/1520-0442\(2002\)015](https://doi.org/10.1175/1520-<br/>527 0442(2002)015), 2002.

528 Reynolds, R. W., Smith, T. M., Liu, C., Chelton, D. B., Casey, K. S., and Schlax, M. G.: Daily high-  
529 resolution-blended analyses for sea surface temperature, *Journal of Climate*, 20, 5473-5496,  
530 <https://doi.org/10.1175/2007JCLI1824.1>, 2007.

531 Robinson, C. J.: Evolution of the 2014–2015 sea surface temperature warming in the central west coast of  
532 Baja California, Mexico, recorded by remote sensing, *Geophysical Research Letters*, 43, 7066-7071,  
533 <https://doi.org/10.1002/2016GL069356>, 2016.

534 Shakun, J. D., and Shaman, J.: Tropical origins of North and South Pacific decadal variability, *Geophysical  
535 Research Letters*, 36, L19711, <https://doi.org/10.1029/2009GL040313>, 2009.

536 Shaltout, M., and Omstedt, A.: Recent sea surface temperature trends and future scenarios for the  
537 Mediterranean Sea, *Oceanologia*, 56, 411-443, <https://doi.org/10.5697/oc.56-3.411>, 2014.

538 Skirving, W., Enríquez, S., Hedley, J.D., Dove, S., Eakin, C.M., Mason, R.A.B., De La Cour, J.L., Liu,  
539 G., Hoegh-Guldberg, O., Strong, A.E., Mumby, P.J., and Iglesias-Prieto, R.: Remote Sensing of Coral



540        Bleaching Using Temperature and Light: Progress towards an Operational Algorithm, *Remote  
541        Sensing*, 10, 18, <https://doi.org/10.3390/rs10010018>, 2018.

542        Skliris, N., Sofianos, S., Gkanasos, A., Mantzafou, A., Vervatis, V., Axaopoulos, P., and Lascaratos, A.:  
543        Decadal scale variability of sea surface temperature in the Mediterranean Sea in relation to  
544        atmospheric variability, *Ocean Dynamics*, 62, 13-30, <https://doi.org/10.1007/s10236-011-0493-5>,  
545        2012.

546        Smith, C. A., Compo, G. P., and Hooper, D. K.: Web-Based Reanalysis Intercomparison Tools (WRIT)  
547        for analysis and comparison of reanalyses and other datasets, *Bulletin of the American  
548        Meteorological Society*, 95, 1671-1678, <https://doi.org/10.1175/BAMS-D-13-00192.1>, 2014.

549        Smith, T. M., Reynolds, R. W., Peterson, T. C., and Lawrimore, J.: Improvements to NOAA's historical  
550        merged land-ocean surface temperature analysis (1880–2006), *Journal of Climate*, 21, 2283-2296,  
551        <https://doi.org/10.1175/2007JCLI2100.1>, 2008.

552        Stuecker, M. F., Jin, F. F., Timmermann, A., and McGregor, S. Combination mode dynamics of the  
553        anomalous northwest Pacific anticyclone, *Journal of Climate*, 28, 1093-1111,  
554        <https://doi.org/10.1175/JCLI-D-14-00225.1>, 2015.

555        Song, D., Duan, Z., Zhai, F., and He, Q.: Surface diurnal warming in the East China Sea derived from  
556        satellite remote sensing, *Chinese Journal of Oceanology and Limnology*, 36, 620–629,  
557        <https://doi.org/10.1007/s00343-018-7035-7>, 2018.

558        Takakura, T., Kawamura, R., Kawano, T., Ichiyangai, K., Tanoue, M., and Yoshimura, K.: An estimation  
559        of water origins in the vicinity of a tropical cyclone's center and associated dynamic processes,  
560        *Climate Dynamics*, 50, 555-569, <https://doi.org/10.1007/s00382-017-3626-9>, 2018.

561        Tang, D., Kester, D. R., Wang, Z., Lian, J., and Kawamura, H. AVHRR satellite remote sensing and  
562        shipboard measurements of the thermal plume from the Daya Bay, nuclear power station, China,  
563        *Remote Sensing of Environment*, 84, 506-515, [https://doi.org/10.1016/S0034-4257\(02\)00149-9](https://doi.org/10.1016/S0034-4257(02)00149-9),  
564        2003.

565        Tian, F., von Storch, J. S., and Hertwig, E.: Impact of SST diurnal cycle on ENSO asymmetry[J]. *Climate  
566        Dynamics*, 52, 2399–2411, <https://doi.org/10.1007/s00382-018-4271-7>, 2019.

567        Trenberth, K. E., and Hurrell, J. W.: Decadal atmosphere-ocean variations in the Pacific, *Climate  
568        Dynamics*, 9, 303-319, <https://doi.org/10.1007/BF00204745>, 1994.

569        Wang, C., Zou, L., and Zhou, T.: SST biases over the Northwest Pacific and possible causes in CMIP5  
570        models, *Science China Earth Sciences*, 61, 1-12, <https://doi.org/10.1007/s11430-017-9171-8>, 2018.

571        Wang, Y., Liu, P., Li, T., and Fu, Y.: Climatologic comparison of HadISST1 and TMI sea surface  
572        temperature datasets, *Science China Earth Sciences*, 54, 1238-1247, <https://doi.org/10.1007/s11430-011-4214-1>, 2011.

574        Wills, R. C., Schneider, T., Wallace, J. M., Battisti, D. S., and Hartmann, D. L.: Disentangling global  
575        warming, multidecadal variability, and El Niño in Pacific temperatures, *Geophysical Research  
576        Letters*, 45, 2487-2496, <https://doi.org/10.1002/2017GL076327>, 2018.



577 Wu, Z., Jiang, C., Deng, B., Chen, J., Long, Y., Qu, K., and Liu, X.: Simulation of Typhoon Kai-tak using  
578 a mesoscale coupled WRF-ROMS model, *Ocean Engineering*, 175, 1-15,  
579 <https://doi.org/10.1016/j.oceaneng.2019.01.053>, 2019a.

580 Wu, Z., Jiang, C., Deng, B., et al. Sensitivity of WRF simulated typhoon track and intensity over the South  
581 China Sea to horizontal and vertical resolutions, *Acta Oceanologica Sinica*, 38(7): 74-83,  
582 <https://doi.org/10.1007/s13131-019-1459-z>, 2019b.

583 Wu, Z., Jiang, C., Chen, J., Long, Y., Deng, B., and Liu, X.: Three-Dimensional Temperature Field Change  
584 in the South China Sea during Typhoon Kai-Tak (1213) Based on a Fully Coupled Atmosphere–  
585 Wave–Ocean Model, *Water*, 11, 140, <https://doi.org/10.3390/w11010140>, 2019c.

586 Wu, Z., Jiang, C., Conde, M., Deng, B., and Chen, J.: Hybrid improved empirical mode decomposition  
587 and BP neural network model for the prediction of sea surface temperature, *Ocean Science*, 15, 349-  
588 360, <https://doi.org/10.5194/os-15-349-2019>, 2019d.

589 Xiao, M., Zhang, Q., and Singh, V. P.: Influences of ENSO, NAO, IOD and PDO on seasonal precipitation  
590 regimes in the Yangtze River basin, China, *International Journal of Climatology*, 35, 3556-3567,  
591 <https://doi.org/10.1002/joc.4228>, 2015.

592 Xu, L., He, S., Li, F., Ma, J., and Wang, H. Numerical simulation on the southern flood and northern  
593 drought in summer 2014 over Eastern China, *Theoretical and Applied Climatology*, 134, 1-13,  
594 <https://doi.org/10.1007/s00704-017-2341-0>, 2018.

595 Xue, X., Chen, W., Chen, S., and Feng, J.: PDO modulation of the ENSO impact on the summer South  
596 Asian high, *Climate Dynamics*, 50, 1393-1411, <https://doi.org/10.1007/s00382-017-3692-z>, 2018.

597 Yamamoto, R., Iwashima, T., and Hoshiai, M.: An analysis of climatic jump, *Journal of the Meteorological  
598 Society of Japan. Ser. II*, 64, 273-281, [https://doi.org/10.2151/jmsj1965.64.2\\_273](https://doi.org/10.2151/jmsj1965.64.2_273), 1986.

599 Yang, L., Chen, S., Wang, C., Wang, D., and Wang, X.: Potential impact of the Pacific Decadal Oscillation  
600 and sea surface temperature in the tropical Indian Ocean–Western Pacific on the variability of  
601 typhoon landfall on the China coast, *Climate Dynamics*, 51, 1-11, <https://doi.org/10.1007/s00382-017-4037-7>, 2017.

603 Yang, J., Gong, P., Fu, R., Zhang, M., Chen, J., Liang, S., Xu, B., Shi, J., and Dickinson, R.: The role of  
604 satellite remote sensing in climate change studies, *Nature climate change*, 3, 875,  
605 <https://doi.org/10.1038/nclimate1908>, 2013.

606 Zhang, C., Li, H., Liu, S., Shao, L., Zhao, Z., and Liu, H.: Automatic detection of oceanic eddies in  
607 reanalyzed SST images and its application in the East China Sea, *Science China Earth Sciences*, 58,  
608 2249-2259, <https://doi.org/10.1007/s11430-015-5101-y>, 2015.

609 Zheng, X. T., Xie, S. P., Lv, L. H., and Zhou, Z. Q.: Intermodel uncertainty in ENSO amplitude change  
610 tied to Pacific Ocean warming pattern, *Journal of Climate*, 29, 7265-7279,  
611 <https://doi.org/10.1175/JCLI-D-16-0039.1>, 2016.

612 Zhou, T., Yu, R., Zhang, J., Drange, H., Cassou, C., Deser, C., Hodson, D. L. R., Sanchez-Gomez E., Li, J.,  
613 Keenlyside, N., Xin, X., and Okumura, Y.: Why the western Pacific subtropical high has extended  
614 westward since the late 1970s, *Journal of Climate*, 22, 2199-2215,  
615 <https://doi.org/10.1175/2008JCLI2527.1>, 2009.